Geomorphology 351 (2020) 106933

Contents lists available at ScienceDirect

Geomorphology

journal homepage: www.elsevier.com/locate/geomorph

Direct observations of a three million cubic meter rock-slope collapse with almost immediate initiation of ensuing debris flows

Fabian Walter[a,*], Florian Amann[b], Andrew Kos[c], Robert Kenner[d], Marcia Phillips[d], Antoine de Preux[e], Matthias Huss[a,f], Christian Tognacca[g], John Clinton[h], Tobias Diehl[h], Yves Bonanomi[i]

[a] Laboratory of Hydraulics, Hydrology and Glaciology (VAW), ETH Zurich, Zurich, Switzerland
[b] Chair of Engineering Geology and Hydrogeology, RWTH Aachen University, Germany
[c] Terrasense Switzerland Ltd, Buchs SG, Switzerland
[d] WSL Institute for Snow and Avalanche Research SLF, Davos, Switzerland
[e] Marti AG, Bern, Switzerland
[f] Department of Geosciences, University of Fribourg, Fribourg, Switzerland
[g] Beffa Tognacca Gmbh, Switzerland
[h] Swiss Seismological Service, ETH Zurich, Zurich, Switzerland
[i] Bonanomi AG, Igis, Switzerland

ARTICLE INFO

Article history:
Received 26 June 2019
Received in revised form 29 October 2019
Accepted 30 October 2019
Available online 2 November 2019

Keywords:
Rock avalanche
Debris flows
Permafrost
Environmental seismology

ABSTRACT

Catastrophic collapse of large rock slopes ranks as one of the most hazardous natural phenomena in mountain landscapes. The cascade of events, from rock-slope failure, to rock avalanche and the near-immediate release of debris flows has not previously been described from direct observations. We report on the 2017, 3.0×10^6 m^3 failure on Pizzo Cengalo in Switzerland, which led to human casualties and significant damage to infrastructure. Based on remote sensing and field investigations, we find a change in critical slope stability prior to failure for which permafrost may have played a destabilizing role. The resulting rock avalanche traveled for 3.2 km and removed over one million m^3 of glacier ice and debris deposits from a previous rock avalanche in 2011. Whereas this entrainment did not lead to an unusually large runout distance, it favored debris flow activity from the 2017 rock avalanche deposits: the first debris flow occurred with a delay of 30 s followed by ten debris flows within 9.5 h and two additional events two days later, notably in the absence of rainfall. We hypothesize that entrainment and impact loading of saturated sediments explain the initial mobility of the 2017 rock avalanche deposits leading to a near-immediate initiation of debris flows. This explains why an earlier rock avalanche at the same site in 2011 was not directly followed by debris flows and underlines the importance of considering sediment saturation in a rock avalanche's runout path for Alpine hazard assessments.

1. Introduction

The failure of large rock slopes results in rock avalanches, which can have a long run-out (> 1 km) and charge the landscape with vast quantities of fragmented rock debris. As a result, the risk for remobilizing the unconsolidated deposit material as debris flows, triggered by primary factors such as rainfall or earthquakes or secondary factors such as antecedent rain fall or snow melt (Huang and Fan, 2013) dramatically increases, and remains high for some time after rock slope failure (i.e. days to month, depending on seismicity and the type and quantity of water supply to enhance the debris mobility) (Berger et al., 2011; Baer et al., 2017, Frank et al., 2019).

A few case studies suggest a direct transition of rock avalanches into large and destructive debris flows (*e.g.* Hauser, 2002, Plafker and Ericksen, 1978, Petrakov et al., 2008; Huggel, 2009). Hauser (2002) analysed the 1987 6.0×10^6 m^3 Cerro Rabicano rock avalanche (Chile). Entrainment of a significant volume of path material consisting of fluvial sediments and 5–10 m of snow cover may have caused a direct transition from a rock avalanche into a debris flow. A similar transition is reported for the earthquake triggered, 1970 rock-ice-avalanche at the north peak of Nevados Huascaran, Peruvian Andes (Plafker and Ericksen, 1978). The transition from the ice-rock avalanche with an initial volume

* Corresponding author.
E-mail address: walter@vaw.baug.ethz.ch (F. Walter).

https://doi.org/10.1016/j.geomorph.2019.106933

of approximately 50–100 $\times 10^6$ m^3 (the ice volume was approximately 5.0 $\times 10^6$ m^3) into a debris flow was likely associated with the entrainment of debris and a significant amount of snow and firn. The accumulated snow depth at the 2.4 km-long transition zone when the rock mass moved across Glacier 511 was estimated to be at least 28 m and the total entrained, equivalent water volume was 10–20 $\times 10^6$ m^3 (Plafker and Ericksen, 1978).

Large rock slopes fail when they reach a critical stress threshold (Kos et al., 2016). Recognising the change in criticality, well in advance of failure however, remains a challenge. Even though the process cascade from slope failure to rock avalanche and debris flow is a recognised phenomenon, the underlying mechanisms controlling the transition remain poorly understood. From published accounts, rock avalanche deposits were either remobilized as debris flows long after the initial rock avalanche event, or events had to be reconstructed via scientific back-analysis (e.g., Marietan, 1925; Evans and Clague, 1994, Kotlyakov et al. (2004), Haeberli et al., 2004; Huggel et al., 2005; Petrakov et al., 2008; Huggel, 2009; Kääb et al., 2018).

Here we focus on the sequence of events before, during and after the massive 2017 rock slope collapse on Pizzo Cengalo in the Swiss Alps. The collapse was observed and documented in unprecedented detail, resulting in a new picture of cascading hazard interactions for large rock slope instabilities. In contrast to other case studies, where debris flows were triggered by earthquakes, rainfall or snow melt long after a rock avalanche (e.g. Berger et al., 2011; Baer et al., 2017) or directly transitioned into a debris flow (e.g. Plafker and Ericksen, 1978, Hauser, 2002), the Pizzo Cengalo rock avalanche was deposited and followed by a first debris flow with a delay of 30 s and in absence of any precipitation. Understanding the factors influencing the observed cascades and the mechanisms behind process interactions is critical for developing future hazard management strategies.

2. Study site and history of rock slope failure

Pizzo Cengalo (WGS 84: 46°17′49.090″N 9°36′37.688″E, 3369 m asl) is situated in the Val Bregaglia region within Eastern Switzerland's Canton Grisons. It locates at the valley head of the Bondasca Valley, some 6 km up-valley from the village of Bondo (Figs. 1 and 2). Near Pizzo Cengalo, the Bondasca Valley and its lateral canyons host a number of small glaciers (Figs. 1 and 2b). At lower altitudes, the valley has been sparsely developed with an access road, vacation homes, stables, popular hiking trails, a seasonally occupied mountain hut ("Sciora Hut") and parking areas.

Pizzo Cengalo's NE face has been subject to varying sizes of rock slope failures. Systematic observation of the rock slope instability commenced in 2012, in response to a 1.5 $\times 10^6$ m^3 rock wall collapse, which occurred in December 2011 (Fig. 2c). The 2011 collapse evolved into a rock avalanche, traveling 2.7 km down the Bondasca valley, and charged the landscape with a considerable deposit of rock debris (Fig. 2c). Photographs show that the back scarp of the 2011 failure was largely covered with a thick layer of blue permafrost ice (Fig. S3a), which may have contributed to the catastrophic failure. During summer 2012, heavy rainfall remobilized parts of the 2011 rock avalanche deposit, and four debris flows were triggered, which reached the village of Bondo, located at a distance of 6 km at the valley bottom (Baer et al., 2017). The debris flow hazard prompted the construction of a retention basin in Bondo and the installation of an early warning system at Prä (Fig. 1).

On 23 August 2017, another, significantly larger rock volume of 3.00 $\times 10^6 \pm$ 0.02 m^3 collapsed at the Pizzo Cengalo NE face, (Figs. 1 and 2d) as determined from repeated terrestrial laser scans (TLS, see Sections 3 and Text S2) and time-laps photographs, which also document a precursory 0.10-0.15 $\times 10^6$ m^3 rock fall event on 21 August 2017 (personal communication M. Keiser, Canton Grisons). The main collapse on 23 August 2017 resulted in a 3.2 km long rock avalanche, which overran the deposits of the 2011 event and reached the hiking trail to the Sciora Hut (Fig. 2d). The rock avalanche claimed the lives of eight hikers who passed the affected trail section at the time of failure.

3. Slope stability prior to the 2017 event

Displacement monitoring with terrestrial radar interferometry (TRI, see Section S3 in the supplementary material for details) and TLS between 2012 and 2017 prompted an early warning issued several weeks prior to the 2017 catastrophic failure. TRI data showed that annual displacements varied between 40 mm yr^{-1} and 60 mm yr^{-1} during the 2012–2015 period (Fig. 4). Between August 2015 and July 2016 annual displacements notably increased by a factor 1.5, and were then followed by a dramatic, factor 2.5–3.0 increase between July 2016 and July 2017. TRI measurements in summer 2013 indicate no slope displacements during the summer season (Fig. 4b–c). Thus, the measured annual displacements accumulated solely between the beginning of fall and end of spring. During this period, increased fluid pressure associated with snow melt infiltration cannot explain the observed displacements, as snow accumulates only at a few locations in the steep rock wall. Additionally, snow melt on North-facing rock slopes tends to form a basal ice layer under the snow pack in spring, largely preventing the infiltration of melt water (Phillips et al. (2016)).

After the 2017 failure, first-hand observations via telescope confirmed small patches of ice in the back scarp, which appeared covered or interspersed with debris and dust. In addition to these observations of ice, a recently developed permafrost distribution map confirms the presence of permafrost in the NE slope of Pizzo Cengalo (Kenner et al., 2019). Permafrost is known to play an important role in rock slope stability (Allen et al., 2013; Krautblatter et al., 2013; Deline et al., 2015; Phillips et al., 2016). Ice segregation or freeze thaw cycles can induce ice growth in fractures (ice-wedging) which enhance crack opening (Matsuoka, 2001; Draebing et al., 2017) followed by progressive rock bridge failure (Phillips et al., 2016). The fact that at least in 2013 displacements were only observed between the beginning of fall and end of spring but not during the summer period suggests that ice-wedging is an important preparatory factor.

The increased displacement rates after 2015 suggest an increase in the degree of criticality (i.e., a greater proportion of discontinuities in the rock mass are close to their strength limit) resulting from rock bridge failure that occurred in the previous years. This is consistent with the TLS data obtained between late spring and early fall 2016, which in contrast to 2013 also showed significant displacements during the summer period. The increased criticality implied an increased sensitivity of the rock slope to stress changes induced, for example, by changes in water pressure associated with summer rainfall events.

The final trigger for the rock slope failure in August 2017 cannot be associated with a single event. Post-failure analysis however shows that at the time of failure, the water levels in daylighting structures at the lateral release surface were approximately 60 m above the basal failure plane (Fig. 3).

The orientation of geological structures is a key controlling factor for the Pizzo Cengalo rock slope instability. Structures in the granodiorite include three penetrative, brittle sets of discontinuities (Fig. 3 and S1 in the Supplementary information). Prior to the 2017 catastrophic failure, kinematic analysis of the geological structures (Supplementary information) indicates a primary toppling mechanism along slope-parallel discontinuities (Set 3 in Fig. 3 and S1). Those discontinuities affect the rock slope stabil-

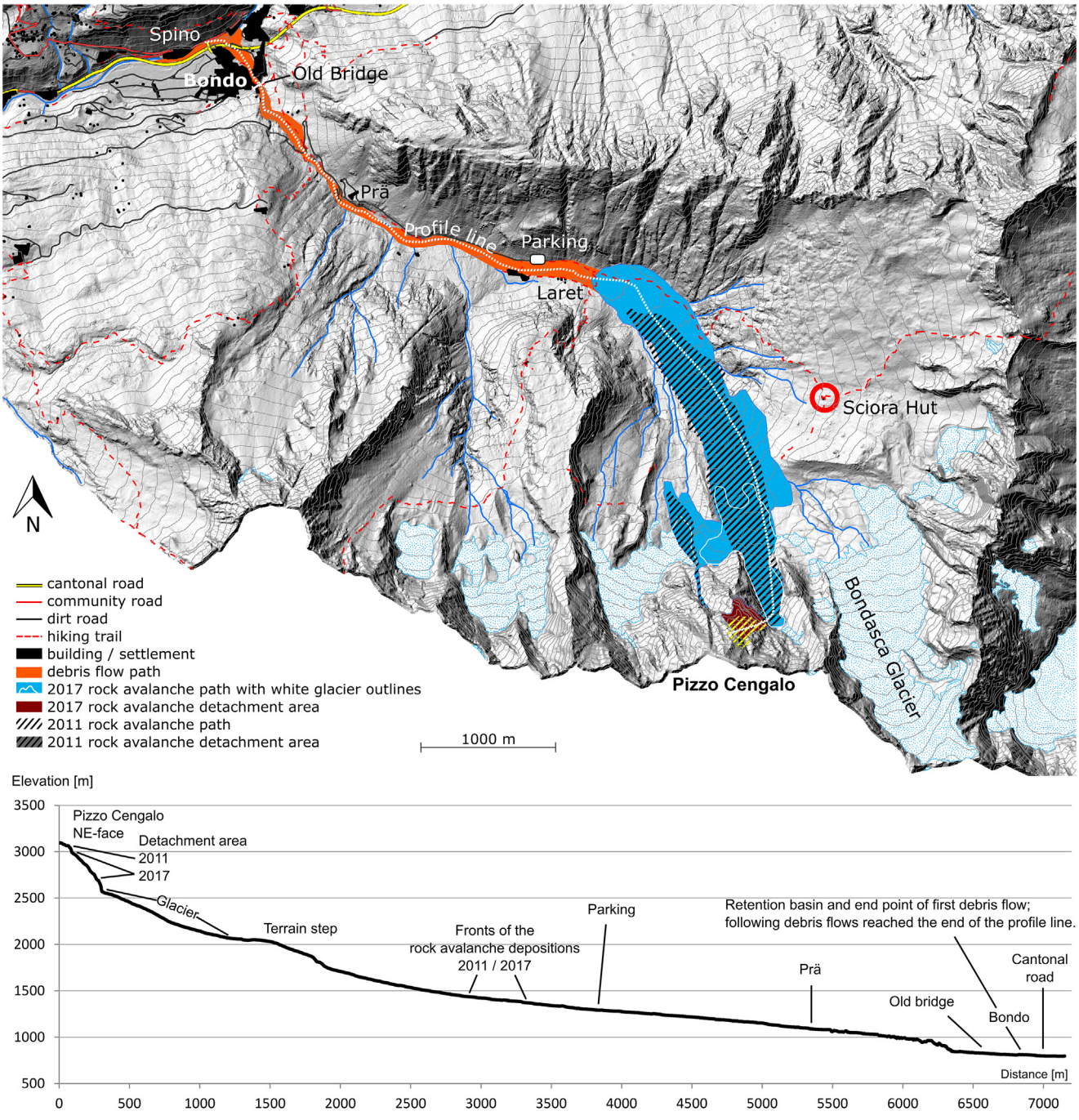

Fig. 1. Overview map and topographic cross section showing the Bondasca Valley, Pizzo Cengalo and the village of Bondo. Limits of the 2011 and 2017 rock avalanche deposits, and limits of the debris flows are also shown. Note the debris flow retention basin in Bondo and an early warning system for debris flows installed at Prä.

ity above 2800 m asl. Below this elevation, the lower dip angle of these discontinuities renders toppling unlikely. This is supported by displacement maps obtained from radar interferometric measurements, which indicate no displacements below 2800 m asl (Fig. 4). Due to toppling, the steep slope-parallel structures (Set 2) are kinematically unconstrained and sliding can occur as a secondary mechanism. Set 1 (Fig. 3c) is of particular importance for the deep-seated rock slope instability because it strikes normal to the slope and, due to its widespread persistence (e.g. > 50 m), forms major lateral release planes (Fig. 3). The basal failure plane of the slope instability is not associated with pre-existing geological structures, but rather exhibits a step-shaped surface indicating progressive rock bridge failure (Fig. 3) (Gischig et al., 2011a, 2011; Phillips et al., 2016). Failure of rock bridges was frequently heard as a low-frequency rumbling during summer field trips between 2015 and 2017. The qualitative intensity of the audible sounds was notably stronger in 2016 and 2017, which anecdotally correlates with the dramatic increase in displacement rates measured with TRI and TLS.

4. Rock avalanche dynamics

The catastrophic collapse on 23 August 2017 was captured on video (video S1; Supplementary information). The footage shows how the failed rock mass impacted a small glacier located at the foot of the slope (Fig. 2b). The impact caused the ejection of a white jet

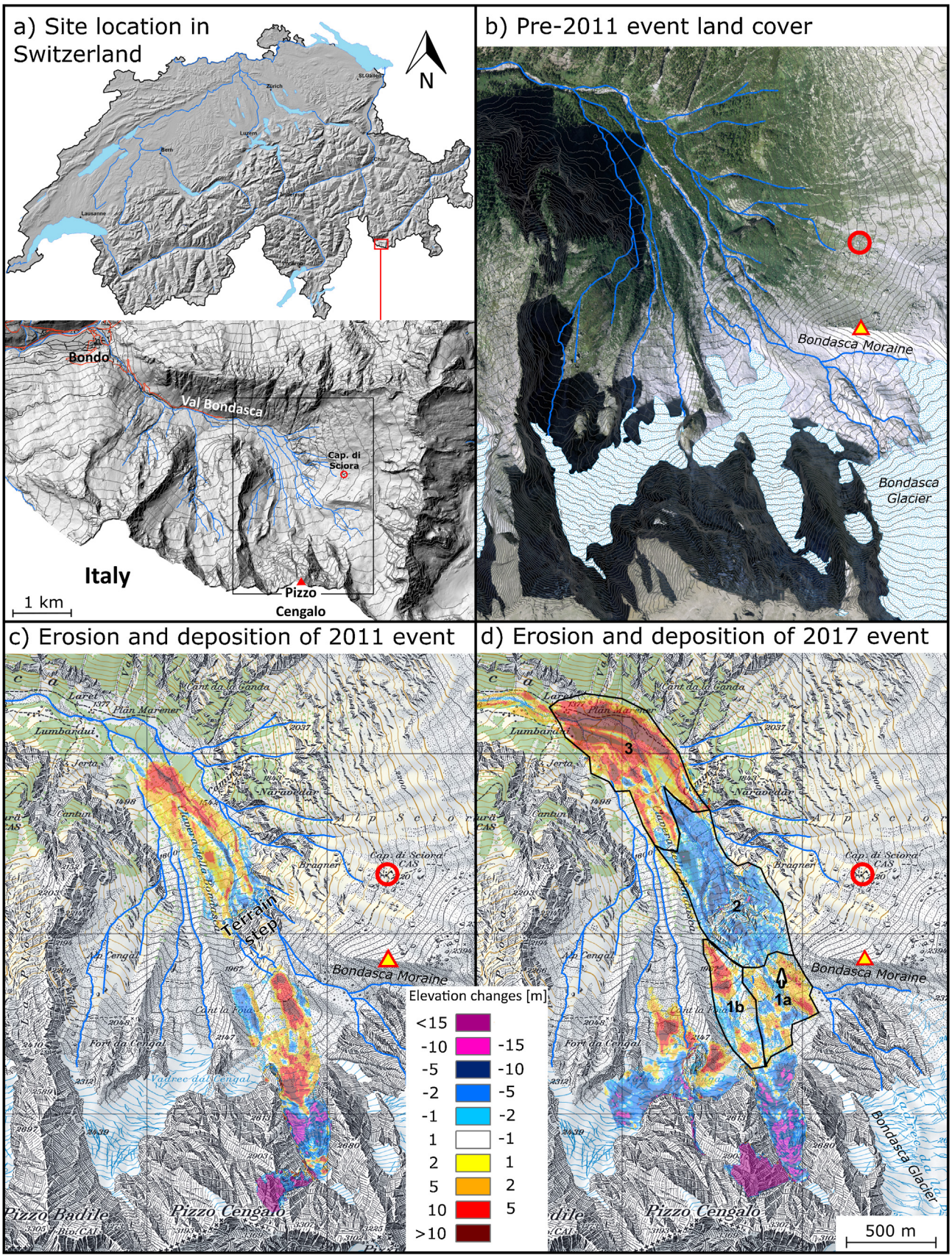

Fig. 2. a) Details of Bondasca Valley head and terrain changes in response to the 2011 and 2017 Pizzo Cengalo rock avalanches. a) Site situation within Switzerland and the Bondasca Valley. b) Glacier coverage and the stream network mapped on an orthophoto which shows Pizzo Cengalo and the upper Bondasca Valley before the 2011 and 2017 rock avalanches. Map data: swissimage© 2019 swisstopo (5704000000). c) & d) Changes in surface elevation caused by the rock slope failures in 2011 and 2017. Map: Swiss Map Raster© 2019 swisstopo (5704 000 000). Red circles in a), b), c) and d): mountain hut Capanna di Sciora. The yellow triangles with a red outline in b), c) and d)

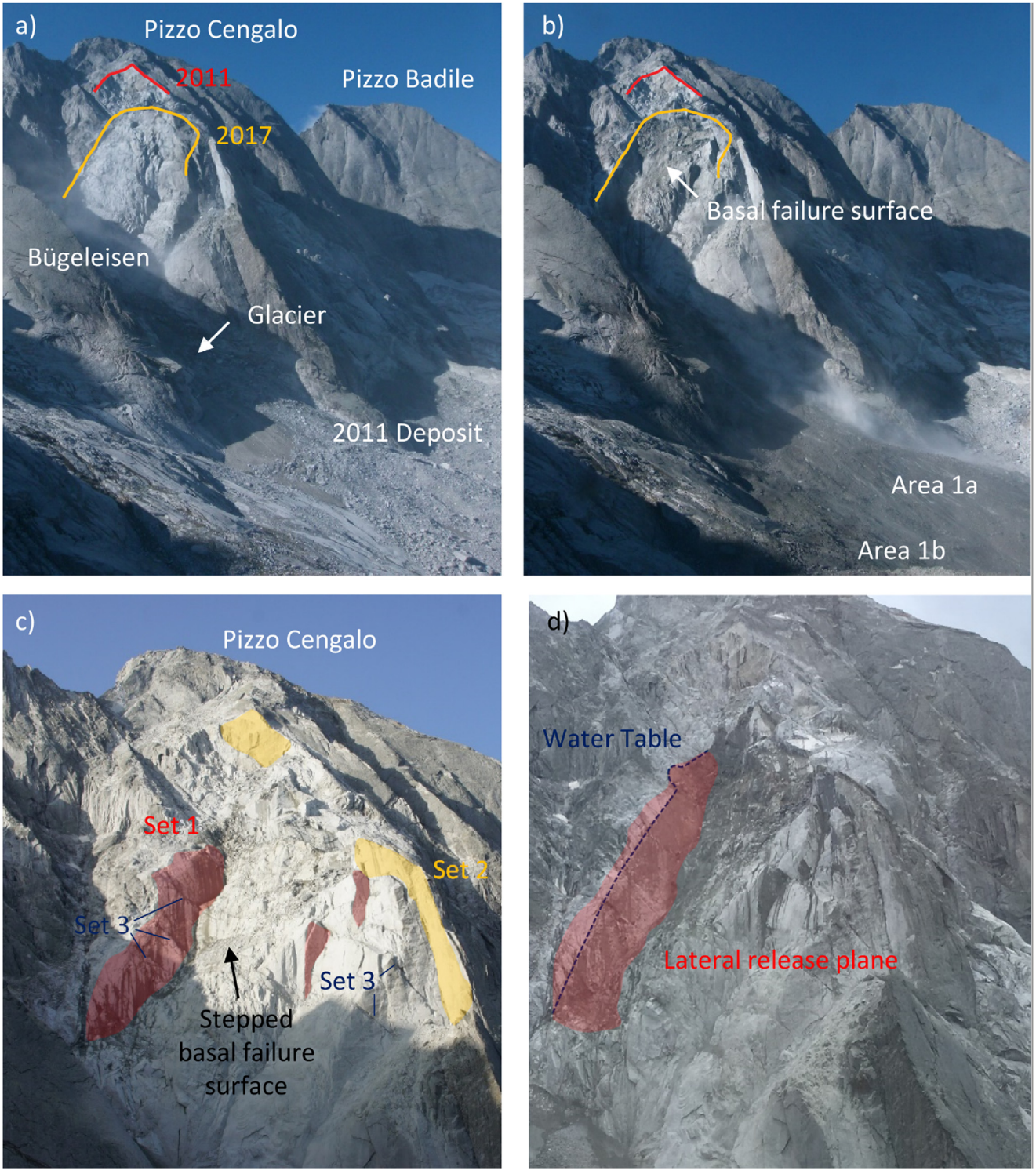

Fig. 3. a) The Pizzo Cengalo NE face before the 2017 rock fall event and b) 6 h after the 2017 failure. The 2011 and 2017 release areas are outlined in red and orange, c) Zoom to the failure zone with the lateral release plane (red) corresponding to Set 1 structures and Set 3 structures (blue) responsible for the primary toppling mechanics and Set 2 structures (orange) that form slope parallel release planes. d) Photograph 48 h after the main rock fall event. The water table can be inferred from water flow from Set 3 structures at the lateral release plane.

indicate the position from which terrestrial laser and radar measurements were carried out. The numbered areas with black outlines in d) define the individual deposition or erosion areas. The white arrow in sector 1a shows the position of the blowholes linked to the occurrence of geyser-like water fountains (Figure S3b). Erosion/deposition distributions are differences of the Federal Office of Topography swisstopo (www.swisstopo.admin.ch) digital elevation models registered on 18 July 2012 - 26 September 2011 (Panel c) and 25 August 2017 - 30 August 2015 (Panel d).

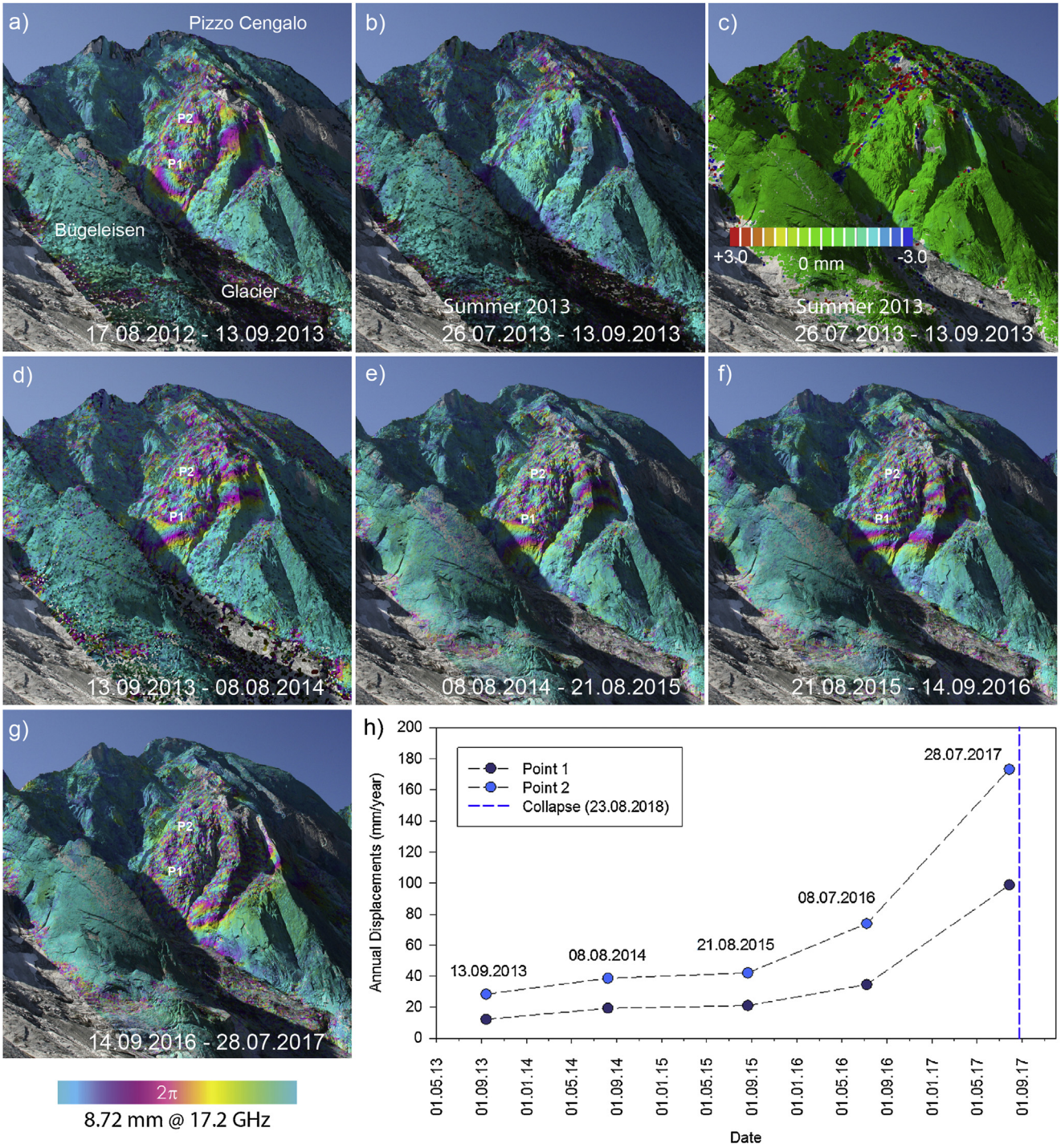

Fig. 4. Results of rock slope displacement monitoring acquired with a portable radar interferometer. Displacements in panels a, b, d – g are shown as interferograms. Each color cycle (e.g., fringe) represents an 8.72 mm displacement and is defined by the wavelength of the radar's central frequency (e.g., 17.2 GHz). c, a phase-unwrapped displacement map, scaled to ±3.0 mm. The interferograms and displacement map were projected into a three-dimensional photogrammetric model for visualization. At points P1 and P2 displacement data were extracted and plotted in panel h. h) yearly displacement rates at two selected points extracted from interferograms between 2012–2017 (P1 and P2). The date of catastrophic failure is shown by the dashed line.

of ice and/or water particles with a sub-vertical trajectory directed towards the W-face of the Bügeleisen ridgeline (Fig. 3a). It was then redirected along a NE trajectory down the Bondasca valley (e.g. in the direction of the rock avalanche run-out Fig. 2). The ice jet was airborne for approximately 8–9 s and the fall-out of the particles occurred along a distance of approximately 450–550 m mainly in area 1a (Fig. 2d). Our first-order approximation from video S1 suggests a velocity of up to 70 m s^{-1} for the larger and faster particles on the leading edge of the ice jet. A volume of $0.6 \pm 0.1 \times 10^6$ m^3 glacier ice was removed by an undetermined combination of melting, impact and erosion (for the volume estimation see Supplementary information).

The cascade of events was recorded on nearby seismic stations, and was equivalent to an earthquake of MI 3.0 (Fig. 5) as reported by the Swiss Seismological Service. At distances exceeding 100 km, seismic stations recorded a broadband signal between 0.005 and

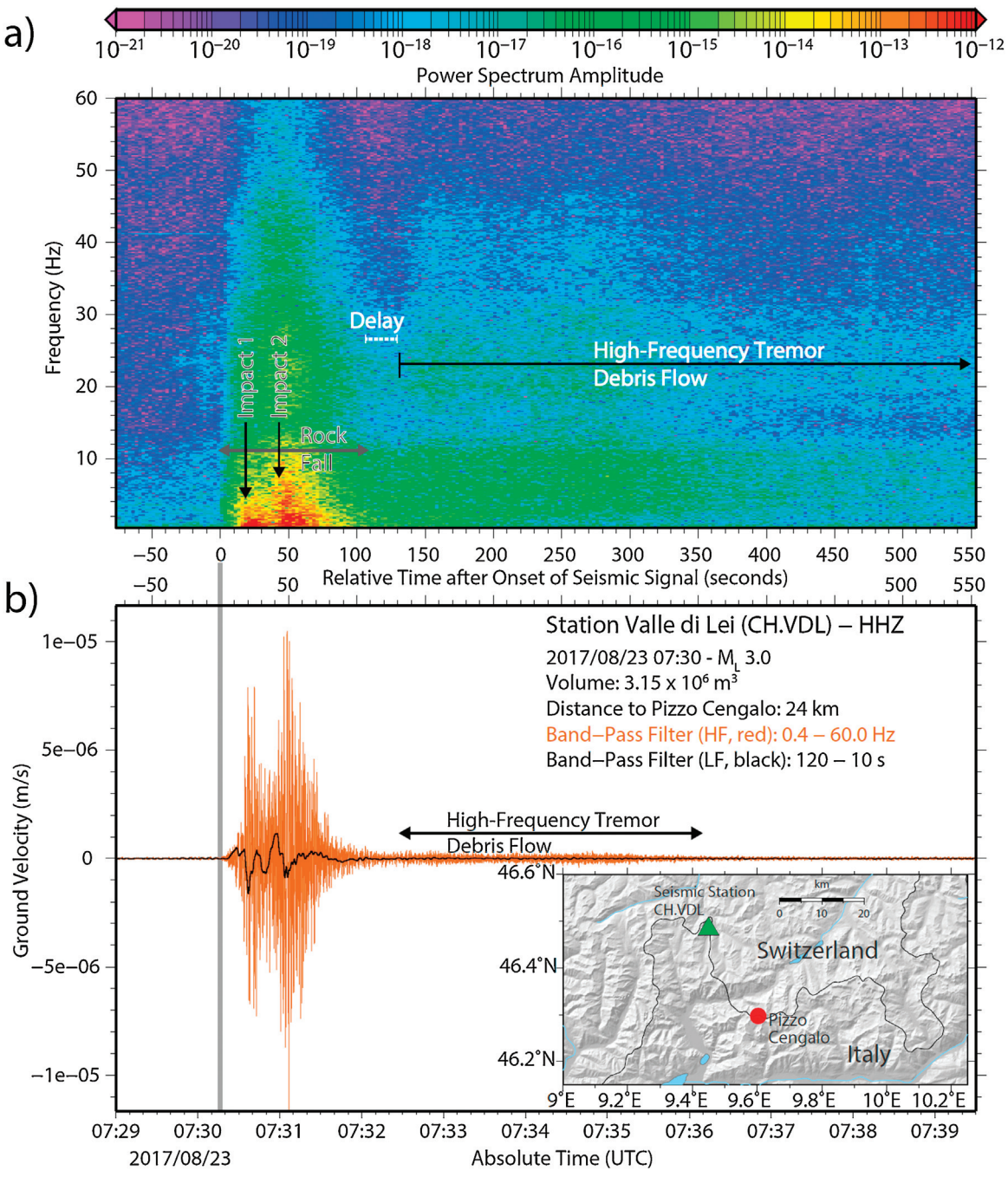

Fig. 5. Spectrogram (top) derived from the ground-velocity seismogram (bottom) of the 2017 rock avalanche event recorded at the closet seismic station CH.VDL (46.48317, 9.44956; Figure S4). A first peak in amplitude occurs about 15–30 s after the first onset of the signal, followed by a larger second peak at about 40–60 s. With a delay of 30 s, the rock avalanche signal is followed by a sustained high-frequency debris flow tremor with initially elevated energy above 20 Hz for at least 200–300 s.

several Hz (Fig. S5), allowing for a detailed reconstruction of the rock avalanche run-out dynamics. Seismic energy above 1 Hz is associated with inter-particle collisions and particle interaction with obstacles in the run-out path, whereas the lower frequencies are caused by the force, which the rock avalanche's bulk motion exerts on the Earth's surface (Ekström and Stark, 2013; Allstadt, 2013; Allstadt et al., 2018, and references therein; see details in Text S8).

Following Allstadt (2013), we invert the low frequency seismograms (Text S8) for the underlying force history (Fig. 6). Upon initial release, the rock mass accelerates downward and eastward and the elastic reaction ("rebound") of Pizzo Cengalo is opposite, i.e. upward and westward (Phase A in Fig. 6). This likely overlapped with the north-sloping glacier impact pushing the ground southward. The mass then accelerates northward across the glacier, which results in a further southward directed rebound force. Within a few tens of seconds, the mass impacts the Bügeleisen ridgeline to the east of the glacier. The ridgeline exerts a westward force on the rock mass forcing it on a more northward trajectory. This implies an eastward reaction force exerted by the rock mass on the ridgeline (Phase B). During the final frictional slowdown, the rock mass pushes the ground primarily north-northwest and downward (Phase C).

From the rock avalanche's force history (Fig. 6) we calculate the center of mass trajectory (Fig. 7; see Text S8 for details). The trajectory bulges somewhat too far eastward than expected from the valley shape. We therefore interpret the trajectory with care confin-

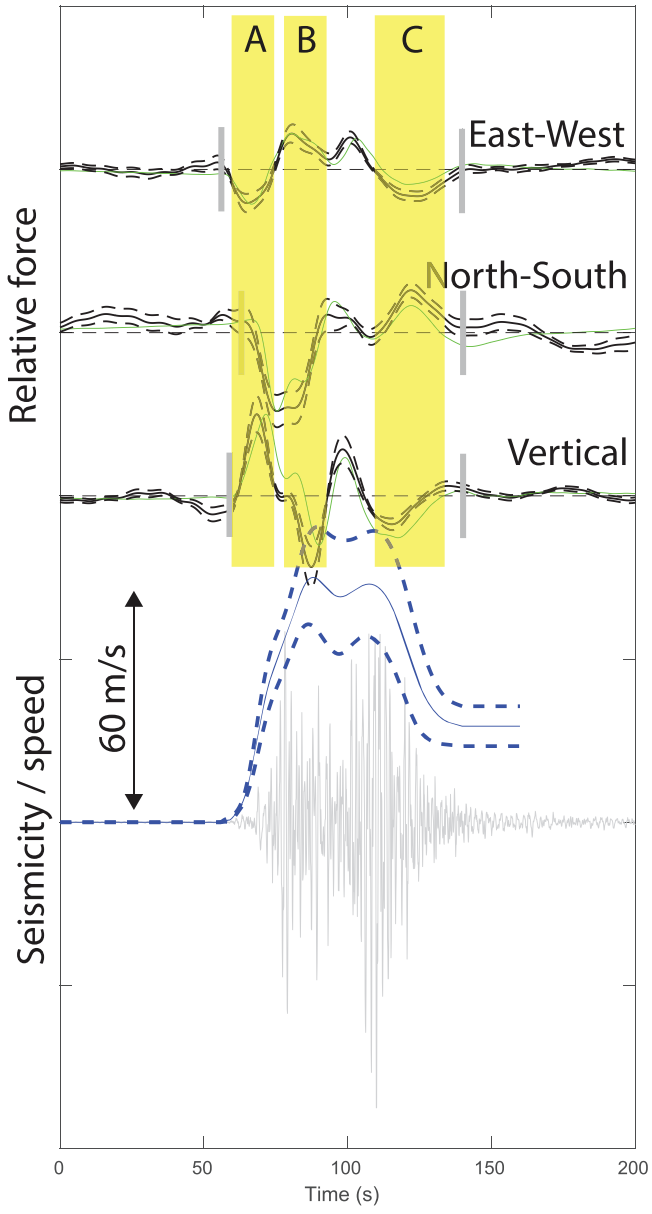

Fig. 6. Force history of the 2017 Pizzo Cengalo rock avalanche. Dashed lines represent uncertainty estimates. Green lines are the low-frequency (0.006 – 0.1 Hz) seismograms from the nearest broadband station VDL (Figure S4). Blue solid line represents the calculated rock avalanche speeds along its trajectory with dashed lines indicating uncertainties. The grey seismogram is the VDL record filtered between 1 and 5 Hz. Different trajectory phases discussed in the main text are labeled (A: mass detachment and glacier impact, B: impact with Bügeleisen ridgeline, C: final slowdown). Vertical grey bars denote the manually picked onset and end of the force history.

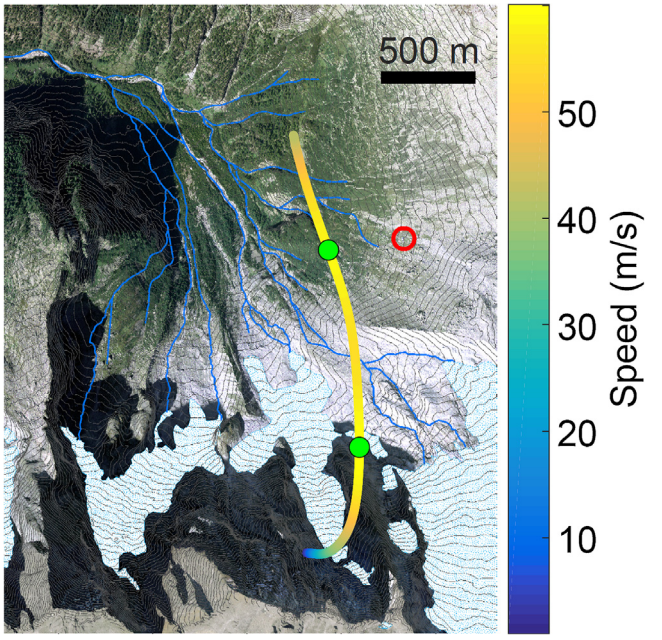

Fig. 7. Rock avalanche trajectory from the force history calculation with center of mass speed color coded. The two green dots indicate speed maxima and the red circle denotes the mountain hut Capanna di Sciora. As calculated rock avalanche speed does not vanish at the end, the calculated trajectory was truncated.

ing a quantitative discussion to those aspects that can be explained with topographic features along the trajectory.

The first of the two avalanche's speed maxima (Figs. 6C and 7) is reached as the center of mass leaves the steep glacier portion and enters flatter terrain (Fig. 2). The second maximum (Figs. 6C and 7) locates just behind the steep terrain step in the central runout area (Figs. 1 and 2). The rock avalanche's high-frequency seismogram exhibits two bursts separated by 20–30 s (Figs. 5 and 6) and the first burst is associated with the glacier impact before the first speed maximum whereas the second high-frequency burst results from the impact behind the downstream terrain step (Figs. 6C and 7).

The timing of high-frequency energy transmission and rock avalanche dynamics is consistent with previous studies: A delay between the high-frequency seismic signal after the rock mass detachment manifesting itself in the start of the force history can be explained with progressive fragmentation of the rock mass (Allstadt, 2013; Hibert et al., 2014]. Similarly, a correspondence of high rock mass momentum and high-frequency seismic signals has been observed for other events (Hibert et al., 2017). However, the generation of the first high-frequency seismic burst of the Piz Cengalo event is likely also related to the collision with the Bügeleisen ridgeline, constituting a topographical barrier (Hibert et al., 2014).

We use the temporal separation of the high-frequency bursts (20–30 s) and the distance between the two ground impact points along the trajectory (about 1200 m), to estimate the rock avalanche's speed between the first and second impact points to 40–60 m s^{-1}. This range of values is consistent with the average speed (Fig. 6), calculated as follows: We integrate the speed time series between the two high-frequency bursts and divide it by the time difference, which gives 44-64 m s^{-1}. About 60 s after the first impact the rock avalanche came to a stop with most of the debris deposited in Area 3 (Fig. 2).

In our inversion of the low-frequency seismic signal the rock avalanche's force history is only constrained by seismic data. As a consequence, those portions of the acceleration and deceleration phases which happen slowly enough to suppress a measurable seismic signal (especially during the final slowdown), are not included in the inverted force history and calculated trajectory. This explains the non-vanishing final rock avalanche speed of 26 m/s (Fig. 6) calculated with our inverted force history. This problem could be mitigated with the inversion algorithm of Ekström and Stark (2013), which requires stationarity of the rock mass' bulk momentum. Moreover, such constrained inversions avoid spurious force histories for band-limited seismic signals (Hibert et al., 2015). For the Piz Cengalo event we follow the unconstrained inversion approach of Allstadt (2013) in order to elucidate dynamic details of the rock avalanche and therefore maximize the bandwidth of the inverted low-frequency seismic signals (Text S8).

5. From rock avalanche to remobilization of rock debris

Within 8.5 days, a series of 15 debris flows formed from the deposits of the 2017 rock avalanche as documented by eye witness observations and seismic data from station VDL (personal communication M. Keiser, Canton Grisons, Fig. 5 and S4; Table S1). The events started nearly immediately after the 2017 rock avalanche. The exact number of individual events is somewhat subjective because it is sometimes not clear whether subsequent surges belonged to the same debris flow. In fact, the first debris flow was overtaken by the second debris flow.

By comparing digital elevation models (DEMs) we estimated the volumes of the single debris flow events. As only four relevant DEMs are available (30.08.2015, 25.08.2017, 30.08.2017 and 05.09.2017; Text S4) only cumulative volumes of successive debris flows can be calculated. Volume estimates for single events relied at least partially on indirect evidence. For example, the geometry of the channel carved by a debris flow was used in its flow volume calculation.

A large debris flow with an initial volume of approximately $0.545 \pm 0.05 \times 10^6$ m^3 was initiated with a delay of approximately 30 s (Fig. 5; see Text S9) after the deposition of the rock avalanche. This event was followed by ten debris flows within 9.5 h and another two debris flows two days after rock avalanche deposition (Table S1). Notably, remobilization of the debris within these two days occurred in the absence of rainfall. A week after the rock avalanche, two debris flows occurred during precipitation on 31 August 2017.

Direct observations show that the first debris flow was a highly viscous, slow moving phenomenon. The initial velocity of the first debris flow was approximately 8 m/s and can be reconstructed from the initiation time derived from the seismic data analysis and the triggering time of the early warning system in "Prä" (Fig. 1) at 09:35:36 UTC on 23 August 2017 (local time is UTC+2 h). The debris flow was first time seen and photographed at around 09:43 close to the exit of the Bondasca valley, about 950 m downstream of the early warning system. These observations suggest an average velocity of 2 m/s. Eye witnesses reported that the debris flow was moving below walking speed when it arrived at the old bridge at 09:48 (average velocity around 0.4 m/s) and it was overtaken by the following debris flow (Table S1). This first debris flow destroyed eleven stables and vacation homes in the Bondasca valley (Fig. 1 and Table S1 in the Supplementary information).

Approximately one hour after the rock avalanche, helicopter-borne observations of a distinct channel in the rock avalanche deposition indicate that the first debris flow originated from Area 3 (Fig. 2d). This first event has a typical debris flow seismogram showing a sustained tremor after the rock avalanche signal with high frequencies up to 50 Hz (Fig. 5) (Allstadt et al., 2018). In the spectrogram (Figs. 5 and S7) the signal mostly resides below 10 Hz and towards its beginning seismicity between 15 and 50 Hz is elevated for 3–4 minutes. A spectral gap above 10 Hz ("delay" in Figs. 5 and S7) clearly separates the rock avalanche seismogram from this initiation signal (Text S9). This shows that the first debris flow formed with a delay of around 30 s after the rock avalanche was deposited (Fig. 5, Table S1). Observations from the helicopter show 12 additional debris flows on 23 and 25 August that reached the retention basin in Bondo (Table S1 and Fig. 1). In contrast to the first debris flow they had a lower viscosity and were initiated from Area 1a (Fig. 2d).

The total volume of the ten debris flows following the first major one on 23 August 2017 was $2.20–2.3 \times 10^5$ m^3. The first eight debris flows did not cause damage in the village of Bondo, but successively filled the debris flow retention basin. Subsequent debris flows overtopped the retention basin and damaged the cantonal road and houses in the village of Bondo. The total volume of debris flows reaching Bondo on 25 August 2017 was $7.0\text{-}8.5 \times 10^4$ m^3. The transported debris again overtopped the retention basin and areas of Bondo were overrun, causing further damage. None of the debris flows caused human casualties. Finally, on 31 August heavy precipitation triggered two debris flows with total volumes of between 2.6 and 2.85×10^5 m^3.

6. Discussion

Our observations reveal the following details about the 2017 rock avalanche:

1 **Detachment:** Rock bridge failure lead to enhanced displacement rates and a critical stability state in the Pizzo Cengalo's NE rock face (Figs. 3 and 4). Ice wedging may have contributed to rock bridge failure.
2 **Dynamics:** The rock avalanche was constrained by ridgelines, slope breaks and other topographical features (Fig. 6), it eroded ca. 0.6×10^6 m^3 of glacial ice (Fig. S2) and produced deposits that covered those of the 2011 rock avalanche and other pre-existing valley fills such as moraines and alluvial fans (Fig. 2).
3 **Immediate debris flows:** Within half a minute to several days after the 2017 rock avalanche, a series of 15 debris flows were mobilized in deposits above and below the terrain step along the rock avalanche's runout path (Fig. 2, Table S1), most of them in the absence of precipitation.

We now address the key question about what caused the high mobility of the 2017 rock avalanche deposits leading to near-immediate formation of the first debris flow in Area 3 (Fig. 2), a terrain inclined only moderately at around 13° (Fig. 1).

The initiation of debris flows requires relatively high water content (e.g. Johnson and Sitar, 1990). A puzzling question in this case is: Where did the water come from to mobilize the debris flows in the absence of precipitation? The water content in the rock slope is volumetrically negligible, and the pore spaces within the disintegrated rock avalanche material are essentially dry. Furthermore, volume expansion as the rock mass disintegrates prohibits pore pressure increase during the dynamic flow (Hungr and Evans, 2004).

The rock avalanche eroded 6.0×10^5 m^3 of glacier ice. Much of this mass likely melted immediately upon rock avalanche impact and during subsequent transport within the rock avalanche. This is supported by accounts of rescue teams searching for the eight missing hikers, hours after the event, who did not report any ice in the deposits (personal communication M. Keiser, Canton Grisons). However, the observed ice/water jet, formed by the initial impact on the glacier (supplemental video), shows that not all of the glacier ice was entrained at the moving front of the rock avalanche: Comparing the average rock avalanche speed calculated from the low frequency seismicity (44–64 m s^{-1}, Section 4) with the speed of the fastest ice jet particles (70 m s^{-1}, Section 4) suggests that the majority of jet ice, which moved much slower than its front, was strewn across the upper surface of the rock avalanche where it subsequently melted and contributed to a higher water content in the deposited rock avalanche debris, thus contributing to its mobility (Area 3 in Fig. 2).

Apart from the lost glacier ice, Fig. 2 shows a distinct pattern of material erosion and deposition during the 2017 rock avalanche: Above the topographic step, debris was deposited in Area 1 between the toe of the Pizzo Cengalo and the Bondasca moraine to the East (Fig. 2). Between Areas 1 and 3, in Area 2, erosion and thus entrainment of sediments occurred during the rock avalanche run-out (Fig. 2). We focus on areas showing deposition in 2011 and erosion in 2017 to specifically quantify the

amount of entrained material from the 2011 deposit in the 2017 rock avalanche. DEM differences (Fig. 2) show that thickness of the 2011 deposits locally exceeded 10 m and at least 6.65×10^5 m^3 of these deposits were eroded and entrained by the 2017 event.

In addition to the entrainment of 6.65×10^5 m^3 of the 2011 rock avalanche deposit, DEM differencing yields some 2.0×10^5 m^3 of other sediments that have been entrained along the run-out path. These estimates are subject to large uncertainties because the additional sediments were covered by vegetation before the 2017 rock avalanche. Our estimate of the total entrainment volume ranges between 8.0 and 9.0×10^5 m^3 and is considered a lower bound because sediment replacement cannot be excluded. Our analysis shows that entrainment occurred to some extent in Area 1 but mainly in Area 2 (Fig. 2d). Consequently, deposits in Area 3, where the first debris flow was initiated, included much of the 2011 deposits.

Quantitative studies (e.g. Hungr and Evans, 2004; Mangeney et al., 2007, Crosta et al. 2009, Aaron et al., 2019) suggest that entrainment of saturated sediments along the rock avalanche run-out path can enhance the rock avalanche mobility. The rock avalanche mobility is commonly expressed by the index H/L (i.e. the ratio of fall height to horizontal travel distance). Interestingly, the H/L ratio for the 2017 Pizzo Cengalo rock avalanche, with a fall height of H = 1.7 km and a horizontal travel distance of L =3.3 km to the most distal point of Area 3 is 0.53. This H/L ratio is within the range of rock avalanches of similar volumes in non-glaciated areas, with negligible sediment entrainment (Hungr and Evans, 2004; Sosio et al., 2012), and close to a value of 0.6 for dry, fragmented rock, as suggested by Heim (1932). Thus, the H/L ratio indicates that entrainment did not significantly enhance the mobility of the rock avalanche that came to a halt in Area 3, 30 s before the first debris flow was initiated, as shown by the seismic frequency signature (Text S9, Fig. S7). We propose, however, that the *water content* of the entrained sediments was a critical factor in the *deposit mobility* contributing to the initiation of debris flows in the absence of precipitation.

The surface hydrology prior to the 2017 event (Fig. 2) shows that melt water from the Bondasca glacier drained through the pre-existing sediments (including the 2011 deposits) which were likely saturated at the time of the 2017 rock avalanche. Once entrained in the 2017 rock avalanche, these sediments provided a major source of water. Unlike the entrainment of glacier ice, which at least partially occurred behind the rock avalanche front, much of the saturated sediments were entrained in Area 2 and deposited in Area 3, where the first debris flow initiated.

The first-hand accounts of climbers who coincidentally witnessed the event, reported that in Area 1a (Fig. 2), geyser-like water fountains (blowouts) occurred 25 and 40 min after the rock avalanche (Fig. S3). The climbers reported two explosive and clearly audible water fountains with an estimated height of a few meters. The remnants of the blowouts were located later in the field by the authors (location shown by an arrow in Fig. 2d). Hours later rescue teams reported saturated mud holes adjacent to solid debris deposits along the margins of Area 3 (Fig. 2), which persisted for many days after the event. These observations not only corroborate the presence of water in the 2017 deposits, but also suggest that this water was pressurized and may have diffused to the earth surface where it formed mud holes. We hypothesize that dynamic loading upon impact (Hutchinson and Bahndari, 1971; Bovis and Dagg, 1992; *Hungr an Evans*, 2004) induced the excess pore pressures, which persisted hours to days as a result of low pressure dissipation rates (e.g. Major and Iverson, 1999, and references therein). The resulting mobility of the debris material is also supported by direct observations of the initiation of debris flows from Area 1a (Table S1): Shallow-seated mechanical instability within the debris led to a progressive volume increase of moving debris and eventually to the formation of debris flows. Further, all twelve debris flow events from Area 1a initiated from debris that covered the pre-existing main drainage path of the Bondasca glacier outflow stream (Fig. 2d). The mobility of the debris material was thus additionally enhanced by a continuous sub-surface water supply.

Our hypothesis of entrainment and dynamic loading of water saturated sediments explains why in contrast to the 2017 event, the 2011 rock avalanche was not directly followed by debris flows. Instead, remobilization of the rock avalanche deposit did not occur until six to nine months after the event, in response to heavy summer rainfall in 2012 (Baer et al., 2017). Aerial photographs taken on 26 September 2011 before the 2011 rock avalanche show that the distribution of the sediments in the Bondasca valley was significantly smaller and a greater area of bedrock surfaces was exposed (Fig. 2b). The impact of the failed rock mass eroded only $\sim 0.1 \times 10^6$ m^3 of glacier ice (Text S6) and since the 2011 event occurred in winter, runoff from the Bondasca glacier was negligible. Sediments along the run-out path and in the deposits were therefore likely unsaturated in 2011. The differing mobility between the 2011 and 2017 deposits is in line with laboratory experiments of water-saturated granular flows (Iverson et al., 2011): For flows overriding wet sediments there exists a positive feedback between entrainment and momentum. For flows overriding dry sediments this feedback is negative. Consequently, entrained dry material tends to reduce the run-out distance whereas entrainment of saturated debris can enhance the mobility of the debris (Abele, 1997; Crosta et al., 2009).

From this comparison we recognize that two pre-existing factors played a critical role in the 2017 hazard cascade that ranged from rock wall failure over rock avalanche propagation to ensuing debris flows: 1) The landscape was covered with sufficient sediments from the 2011 rock avalanche, and 2) the pre-existing sediments were saturated with summer melt water from the Bondasca glacier and by intense rainfall during thunderstorms in July and August 2017.

7. Conclusions

This investigation presents a unique opportunity to study a cascade of Alpine mass movement processes. Favored by permafrost conditions, a 3.0×10^6 m^3 rock mass catastrophically failed at the Pizzo Cengalo NE rock face producing a major rock avalanche in fall 2017. Inversion of seismic broadband data yields a force history, which describes dynamic details of the rock avalanche's center of mass trajectory that agrees well with local topographic features like a constraining lateral ridgeline and topographic steps.

Our observations suggest that entrainment and dynamic loading of water saturated sediments may have been dominant factors in the hazard cascade. They did not increase the reach of the 2017 rock avalanche compared to typical non-entraining rock avalanches. However, entrainment of water saturated sediments and the hypothesized dynamic loading may explain the high deposit mobility that caused debris flows nearly immediately after the rock avalanche deposition and in absence of any precipitation. This is in contrast to the 2011 rock avalanche. In 2011 less sediments covered the rock avalanche run-out path which renders entrainment less likely. In addition, the sediments were likely not saturated since the event occurred in winter time with only minimal water run-off from the Bondasca glacier. Saturated sediment entrainment was thus likely the pivotal factor in debris flow production following the 2017 rock avalanche.

The study elucidates the importance of investigating conditions along a rock avalanche runout path when forecasting or assessing hazardous Alpine mass movements. Focusing on conditions in the release zone, only, when estimating timing, volume and runout dis-

tances of rock collapses and ensuing debris flows is insufficient to fully grasp the potential hazard chain downslope, as was shown in the 2017 Pizzo Cengalo event.

Declaration of Competing Interest

The authors declare that they have no known competing financial interests or personal relationships that could have appeared to influence the work reported in this paper.

Acknowledgments

Data are available online at the institutional repository of RWTH Aachen University (http://dx.doi.org/10.18154/RWTH-2018-228255) and the Swiss Seismological Service (http://arclink.ethz.ch/webinterface/). The salary of FW was paid by the Swiss National Science Foundation via Grants PP00P2_157551 and PP00P2_183719). Terrestrial measurements were funded by ArgeAlps. We thank Amandine Sergeant for fruitful discussions on the seismic inversion.

Appendix A. Supplementary data

Supplementary material related to this article can be found, in the online version, at doi:https://doi.org/10.1016/j.geomorph.2019.106933.

References

Aaron, J., McDougall, S., Jordan, P., 2019. Dynamic analysis of the 2012 Johnsons Landing landslide at Kootenay Lake, BC: the importance of undrained flow potential. Can. Geotech. J. (ja).
Abele, G., 1997. Rockslide movement supported by the mobilization of groundwater-saturated valley floor sediments. Zeitschrift fur Geomorphologie 41 (1), 1–20.
Allen, S., Huggel, C., 2013. Extremely warm temperatures as a potential cause of recent high mountain rockfall. Glob. Planet. Change 107, 59–69.
Allstadt, K., 2013. Extracting source characteristics and dynamics of the August 2010 Mount Meager landslide from broadband seismograms. J. Geophys. Res. Earth Surf. 118 (3), 1472–1490.
Allstadt, K.E., Matoza, R.S., Lockhart, A., Moran, S.C., Caplan-Auerbach, J., Haney, M., Thelen, W.A., Malone, S.D., 2018. Seismic and acoustic signatures of surficial mass movements at volcanoes. J. Volcanol. Geotherm. Res.
Baer, P., Huggel, C.H., McArdell, B.W., Frank, F., 2017. Changing debris flow activity after sudden sediment input: a case study from the Swiss Alps. Geol. Today 33 (6), November–December 2017.
Berger, C., McArdell, B.W., Schlunegger, F., 2011. Sediment transfer patterns at the Illgraben catchment, Switzerland: implications for the time scales of debris flow activities. Geomorphology 125 (421–432), 2011.
Bovis, M.J., Dagg, R., 1992. Debris flow triggering by impulsive loading: mechanical modelling and case studies. Can. Geotech. J. 29, 345–352.
Crosta, G.B., Imposimato, S., Roddeman, D., 2009. Numerical modelling of entrainment/deposition in rock and debris-avalanches. Eng. Geol. 109 (1–-2), 135–145.
Deline, P., Gruber, S., Delaloye, R., Fischer, L., Geertsema, M., Giardino, M., et al., 2015. Ice loss and slope stability in high-mountain regions. In: Snow and Ice-related Hazards, Risks and Disasters. Academic Press, pp. 521–561.
Draebing, D., Krautblatter, M., Hoffmann, T., 2017. Thermo-cryogenic controls of fracture kinematics in permafrost rockwalls. Geophys. Res. Lett. 44, 3535–3544.
Ekström, G., Stark, C.P., 2013. Simple scaling of catastrophic landslide dynamics. Science 339 (6126), 1416–1419.
Evans, S.G., Clague, J.J., 1994. Recent climatic change and catastrophic geomorphic processes in mountain environments. Geomorphol. Nat. Hazards, 107–128.
Frank, F., Huggel, C., McArdell, B.W., Vieli, A., 2019. Landslides and increased debris-flow activity: a systematic comparison of six catchments in Switzerland. Earth Surf. Processes Landforms 44 (3), 699–712.
Gischig, V.S., Moore, J.R., Evans, K.F., Amann, F., Loew, S., 2011a. Thermomechanical forcing of deep rock slope deformation: 1. Conceptual study of a simplified slope. J. Geophys. Res. Earth Surf. 116 (F4), F04010.
Gischig, V., Amann, F., Moore, J.R., Loew, S., Eisenbeiss, H., Stempfhuber, W., 2011b. Composite rock slope kinematics at the current randa instability, Switzerland, based on remote sensing and numerical modeling. Eng. Geol. 118 (1–2), 37–53.
Haeberli, W., Huggel, C., Kääb, A., Zgraggen-Oswald, S., Polkvoj, A., Galushkin, I., et al., 2004. The Kolka-Karmadon rock/ice slide of 20 September 2002: an extraordinary event of historical dimensions in North Ossetia, Russian Caucasus. J. Glaciol. 50 (171), 533–546.
Hauser, A., 2002. Rock avalanche and resulting debris flow in Estero Parraguirre and Rio Colorado, region metropolitana, Chile. Geol. Soc. Am. XV, 135–148.
Heim, A., 1932. Bergsturz und Menschenleben (Landslides and Human Lives). Translated by N. Skermer Bitech Press, Vancouver, 1932.
Hibert, C., Ekström, G., Stark, C.P., 2014. Dynamics of the Bingham Canyon Mine landslides from seismic signal analysis. Geophys. Res. Lett. 41 (13), 4535–4541.
Hibert, C., Stark, C.P., Ekström, G., 2015. Dynamics of the Oso-Steelhead landslide from broadband seismic analysis. Nat. Hazards Earth Syst. Sci. 15 (6), 1265–1273.
Hibert, C., Ekström, G., Stark, C.P., 2017. The relationship between bulk-mass momentum and short-period seismic radiation in catastrophic landslides. J. Geophys. Res. Earth Surf. 122 (5), 1201–1215.
Huang, R., Fan, X., 2013. The landslide story. Nat. Geosci. 6, 325–326, http://dx.doi.org/10.1038/ngeo1806, 2013.
Huggel, C., 2009. Recent extreme slope failures in glacial environments: effects of thermal perturbation. Quat. Sci. Rev. 28 (11–12), 1119–1130.
Huggel, C., Zgraggen-Oswald, S., Haeberli, W., Kääb, A., Polkvoj, A., Galushkin, I., Evans, S.G., 2005. The 2002 rock/ice avalanche at Kolka/Karmadon, Russian Caucasus: assessment of extraordinary avalanche formation and mobility, and application of QuickBird satellite imagery. Nat. Hazards Earth Syst. Sci. 5 (2), 173–187.
Hungr, O., Evans, S.G., 2004. Entrainment of debris in rock avalanches: an analysis of long run-out mechanism. GSA Bull. 116 (9/10), 1240–1252, September / October, 2004.
Hutchinson, J.N., Bahndari, R.K., 1971. Undrained loading, a fundamental mechanism of mudflow and other mass movements. Geotechnique 21 (4), 353–358.
Iverson, R.M., Reid, M.E., Logan, M., LaHusen, R.G., Godt, J.W., Griswold, J.P., 2011. Positive feedback and momentum growth during debris-flow entrainment of wet bed sediment. Nat. Geosci. 4 (2), 116.
Johnson, K.A., Sitar, N., 1990. Hydrologic conditions leading to debris-flow initiation. Can. Geotech. J. 27 (6), 789–801.
Kääb, A., Leinss, S., Gilbert, A., Bühler, Y., Gascoin, S., Evans, S.G., et al., 2018. Massive collapse of two glaciers in western Tibet in 2016 after surge-like instability. Nat. Geosci., 1.
Kenner, R., Noetzli, J., Hoelzle, M., Raetzo, H., Phillips, M., 2019. Distinguishing ice-rich and ice-poor permafrost to map ground temperatures and ground ice occurrence in the Swiss Alps. The Cryosphere 13, 1925–1941, http://dx.doi.org/10.5194/tc-13-1925-2019.
Kos, A., Amann, F., Strozzi, T., von Ruette, J., Delaloye, R., Springman, S., 2016. Contemporary glacier retreat triggers a rapid landslide response, Great Aletsch Glacier, Switzerland. Geophys. Res. Lett. 43, http://dx.doi.org/10.1002/2016GL071708, 12‘466–12‘474.
Kotlyakov, V.M., Rototaeva, O.V., Nosenko, G.A., 2004. The September 2002 Kolka glacier catastrophe in North Ossetia, Russian Federation: evidence and analysis. Mountain Res. Dev. 24 (1), 78–83.
Krautblatter, M., Funk, D., Günzel, F.K., 2013. Why permafrost rocks become unstable: a rock–ice-mechanical model in time and space. Earth Surf. Process. Landf. 38 (8), 876–887.
Major, J.M., Iverson, R.M., 1999. Debris-flow deposition: effects of pore-fluid pressure and friction concentrated at flow margins. GSA Bull. 111 (No. 10), 1424–1434, October, 1999.
Mangeney, A., Tsimring, L.S., Volfson, D., Aranson, I.S., Bouchut, F., 2007. Avalanche mobility induced by the presence of an erodible bed and associated entrainment. Geophys. Res. Lett. 34 (22), http://dx.doi.org/10.1029/2007GL031348.
Marietan, I., 1925. Les éboulements de la Cime de l'Est des Dents du Midi en 1926 et le Bois-Noir. Journal Bull. de la Murithienne 44, 67–93, 1925.
Matsuoka, N., 2001. Direct observation of frost wedging in alpine bedrock. Earth Surf. Process. Landf. 26 (6), 601–614, http://dx.doi.org/10.1016/j.coldregions.2016.02.010.
Petrakov, D.A., Chernomorets, S.S., Evans, S.G., Tutubalina, O.V., 2008. Catastrophic glacial multi-phase mass movements: a special type of glacial hazard. Adv. Geosci. 14, 211–218.
Phillips, M., Wolter, A., Lüthi, R., Amann, F., Kenner, R., Bühler, Y., 2016. Rock slope failure in a recently deglaciated permafrost rock wall at Piz Kesch (Eastern Swiss Alps). Earth Surf. Process. Landf., http://dx.doi.org/10.1002/esp.3992, 07/2016.
Plafker, G., Ericksen, G.E., 1978. Nevados Huascaran avalanches, Peru. In Developments in Geotechnical Engineering, Vol. 14. Elsevier, pp. 277–314.
Sosio, R., Croat, G.B., Chen, J.H., Hungr, O., 2012. Moelling rock avalanche propagation on glacier. Quart. Sci. Rev. 47, 23–40, 2012.